Published in final edited form as:
*Adv Mater*. 2009 ; 21(30): 3045–3052. doi:10.1002/adma.200900320.

# Recent Progress in Syntheses and Applications of Dumbbell-like Nanoparticles**

**Chao Wang**,
Department of Chemistry, Brown University, Providence, Rhode Island 02912 (USA)

**Chenjie Xu**,
Department of Chemistry, Brown University, Providence, Rhode Island 02912 (USA)

**Hao Zeng [Prof.]**, and
Department of Physics, University at Buffalo, SUNY, Buffalo, New York 14260 (USA)

**Shouheng Sun [Prof.]**
Department of Chemistry, Brown University, Providence, Rhode Island 02912 (USA)

Chao Wang: ; Chenjie Xu: ; Hao Zeng: haozeng@buffalo.edu; Shouheng Sun: ssun@brown.edu

## Abstract

This paper reviews the recent research progress in syntheses and applications of dumbbell-like nanoparticles. It first describes the general synthesis of dumbbell-like nanoparticles containing noble metal and magnetic NPs/or quantum dots. It then outlines the interesting optical and magnetic properties found in these dumbbell nanoparticles. The review further highlights several exciting application potentials of these nanoparticles in catalysis and biomedicine.

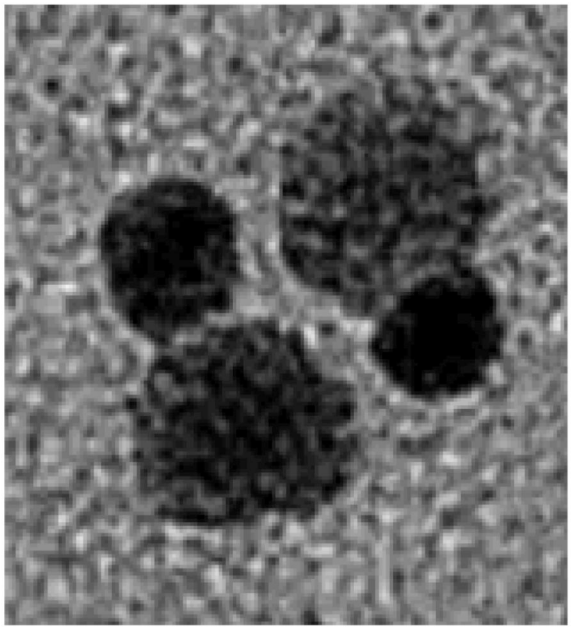

**Work at Brown was support by NSF/DMR 0606264, NIH/NCI 1R21CA12859, and Brown Seed Fund. Work at UB was supported by NSF/DMR 0547036.

Correspondence to: Hao Zeng, haozeng@buffalo.edu; Shouheng Sun, ssun@brown.edu.

**Keywords**

Dumbbell nanoparticles; multifunctional nanoparticles; nanoparticle catalyst; nanomedicine

## 1. Introduction

Dumbbell-like nanoparticles (DBNPs) described in this paper are referred to as those with two different functional NPs in intimate contact, as shown in Figure 1. The interfacial interactions originated from electron transfer across the nanometer contact at the interface of these two NPs can induce new property that is not present in the individual component NPs. For example, gold (Au) NPs are normally chemically inert but Au NPs deposited on a metal-oxide support, a structure similar to what is described in Figure 1, have shown high catalytic activity for CO oxidation.[1] In these Au-oxide composite catalyst systems, the choice of the oxide support plays an important role in the catalysis even thought the oxide is not in nanometer scale. This high activity of Au-oxide catalysts has been rationalized in terms of a junction effect, arising from transfer of electrons from the oxide support to the Fermi level of the adjacent Au NP.[2]

With the example shown in the enhanced catalysis of the Au-oxide catalyst, the importance of studying the dumbbell structure is evident because each side of the NP in the structure is restricted to the nanometer scale and a small variation in electron transfer across the interface between these two limited electron “nanoreservoirs” may lead to drastic property change on each NP. Therefore, DBNPs offer an interesting platform for studying physical and chemical properties of the materials based not only on each NP dimension and shape but also on the communication between the two NPs. Furthermore, magnetically and optically active DBNPs containing two different chemical surfaces are particularly suitable for the selected NP functionalization with both targeting agent and drug molecules, facilitating their applications as multifunctional probes for target-specific imaging and delivery applications.[3]

This report summarizes the recent research progress in preparing and studying DBNPs with interesting optical and magnetic properties. In particular the report focuses on the DBNPs containing noble metal NPs and magnetic NPs or quantum dots (QDs). The nanoscale junctions present in these structures allow electron transfer across the interface, changing the local electronic structure and therefore their physical and chemical properties. These DBNPs offer an ideal nano-system for catalytic and biomedical applications.

## 2. Synthesis of DBNPs

DBNPs are commonly obtained by sequential growth of a second component on the preformed seeds. This is similar to what has been known as the seed-mediated growth to form core/shell NPs but what’s different is that the nucleation and growth is anisotropically centered on one specific crystal plane around the seeding NPs, not uniformly distributed as in the synthesis of core/shell structures. Therefore, the successful synthesis of DBNPs relies critically on promoting the heterogeneous nucleation while suppressing the homogeneous nucleation (i.e. the formation of separate NPs of the second component). This can be achieved by tuning the seed-to-precursor ratio and controlling the heating profile so that the concentration of the precursors is below the homogeneous nucleation threshold throughout the synthesis process.[4] In the growth process, the lattice spacings between two components are generally well-matched to lower the energy required for epitaxial nucleation of the second component.[5] However, lattice mismatch can also be applied to make DBNPs by surface dewetting process in a core/shell structure.[6] Electron transfer at the interface of two components in the

nucleation process may play a key role in controlling the dumbbell morphology and this transfer process can be modulated by the polarity of the solvent.[7]

### 2.1. DBNPs Containing Noble Metal NPs and Magnetic NPs

The two best known examples of the DBNPs containing noble metal NPs and magnetic NPs are Au-$Fe_3O_4$ and Ag-$Fe_3O_4$ NPs.

The Au-$Fe_3O_4$ DBNPs were prepared via the decomposition of iron pentacarbonyl, $Fe(CO)_5$, over the surface of the pre-formed Au NPs followed by oxidation in air, as illustrated in Figure 2a.[7] The Au NPs were either synthesized in situ by injecting $HAuCl_4$ solution into the reaction mixture or pre-made in the presence of oleylamine. Mixing Au NPs with $Fe(CO)_5$ in 1-octadecene solvent in the presence of oleic acid and oleylamine and heating the mixture to reflux (300°C) followed by room-temperature air oxidation led to the formation of Au-$Fe_3O_4$ NPs. The size of the Au NPs was tuned by controlling the temperature at which the $HAuCl_4$ solution was injected, or by controlling the $HAuCl_4$/oleylamine ratio. Injecting the $HAuCl_4$ solution into the reaction mixture containing $Fe(CO)_5$ at higher temperature led to larger Au NPs. The size of the $Fe_3O_4$ NPs was controlled by adjusting the ratio between $Fe(CO)_5$ and Au. More $Fe(CO)_5$ gave larger $Fe_3O_4$ NPs. Figure 2b shows the transmission electron microscopy (TEM) image of the Au-$Fe_3O_4$ DBNPs with $Fe_3O_4$ at around 14 nm and Au at 8 nm. Figure 2c is a typical high-resolution TEM (HRTEM) image of a DBNP with $Fe_3O_4$ at 12 nm and Au at 8 nm. In the structure, a $Fe_3O_4$ (111) plane grows onto an Au (111) plane, giving the dumbbell-like structure.

Similarly, the DBNPs of Pt-$Fe_3O_4$, Pd-$Fe_3O_4$ can be produced by controlled nucleation and growth of Fe on Pt and Pd NPs respectively followed by air oxidation.[8]

The controlled nucleation and growth of only one $Fe_3O_4$ on each Au (or Pt, or Pd) seeding NP in the current synthetic condition is attributed to the possible electron transfer between Au and Fe. In the growth process, $Fe(CO)_5$ decompose into Fe that nucleates on Au NPs. Once the Fe nucleus is formed on Au, the free electrons from Fe tend to flow across the junction to Au. As a result, Au in Au-Fe becomes electron 'rich', unsuitable for multi-nucleation of Fe and giving only the Au-Fe dumbbell structure. When exposed to air, Fe is oxidized to $Fe_3O_4$, forming Au-$Fe_3O_4$ NPs. As seen in the Section 3, the electronic effect across the interface has drastic effects on the optical, magnetic and catalytic properties of these DBNPs.

Different from Au-$Fe_3O_4$ NPs, the Ag-$Fe_3O_4$ NPs were made by controlled nucleation of Ag on the pre-formed $Fe_3O_4$ NPs.[3a] In one synthesis, the as-prepared $Fe_3O_4$ NPs dispersed in organic solution and $AgNO_3$ dissolved in water were mixed and agitated by ultrasonication. The sonication provided the energy required for the formation of a microemulsion with the $Fe_3O_4$ NPs assembling at the liquid/liquid interface. Fe(II) on the NPs acts as catalytic center for the reduction of $Ag^+$ and nucleation/growth of Ag NPs, as illustrated in Figure 3. The partial exposure of the NPs to the aqueous phase caused the formation of DBNPs. However, the inter-particle relation in Ag-$Fe_3O_4$ is not epitaxial as in the Au-$Fe_3O_4$ NPs and therefore the structure show nearly independent surface plasmonic property from Ag and superparamagnetic property from $Fe_3O_4$. This selected nucleation and growth initiated by ultrosonication has also be extended to the synthesis of Ag-FePt and Ag-Au DBNPs.[3a]

Alternatively, Ag-$Fe_3O_4$ can be made by nucleation and growth of Ag on FeS-modified $Fe_3O_4$ NPs.[9] In the synthesis, the $Fe_3O_4$ NPs were first made by reductive decomposition of $Fe(acac)_3$ in phenyl ether and then reacted with hexadecanethiol (1-$C_{16}H_{33}$-SH) at reflux (265° C) in the presence of oleic acid and oleylamine. The HS-group can attach to the iron oxide surface, and at the high reaction temperature, the SH-Fe linkage decomposes to give a thin layer of FeS on the particle surface. The FeS modified $Fe_3O_4$ NPs were then mixed with

$AgNO_3$ in tetralin (1,2,3,4-tetrahydronaphthalene) in the presence of oleylamine. The mixture was heated at 100°C for 1 hour, giving the DBNPs of Ag-$Fe_3O_4$. In this synthesis, the $Fe_3O_4$ size was controlled from the reductive decomposition of iron acetylacetonate, $Fe(acac)_3$, while the size of Ag NPs was tuned by controlling the amount of $AgNO_3$ added in the reaction mixture. Figure 4a–b show the TEM image of two DBNPs aligned in a parallel and anti-parallel configuration, and Figure 4c is the TEM image of an assembly of DBNPs. This controlled nucleation of Ag on FeS-modified $Fe_3O_4$ NP can be readily extended to the synthesis of Ag-$CoFe_2O_4$ and Ag-$MnFe_2O_4$ NPs, offering a general approach to the Ag-$MFe_2O_4$ NPs.[10]

The formation of DBNPs of noble metal with other magnetic NPs is also possible. For example, DBNPs of Au-FePt were synthesized by catalytic growth of Au on FePt NP surface.[11] In the synthesis, the 6 nm FePt NPs were synthesized through a transmetalation reaction between $Fe^0$ and $Pt^{2+}$ precursors. The 6 nm FePt NPs were allowed to react with $AuClPPh_3$ in 1,2-dichlorobenzene containing 1-hexadecylamine, under continuous bubbling of 4% $H_2$/Ar mixture through the solution. The Pt containing NP seeds served as a catalytic surface which activated hydrogen molecules and facilitated the reduction of incoming $Au^+$ to $Au^0$, and the successive growth of Au to the seed resulted in DBNPs of Au-FePt.

More complex DBNPs can be made by fusing the preformed DBNP NPs. An example of $Fe_3O_4$-Au-$Fe_3O_4$ is shown in Figure 5.[12] Such heterostructures were obtained by heating preformed Au-$Fe_3O_4$ NPs in the presence of elemental sulfur (S). In this synthesis, the addition of elemental S is critical to dumbbell formation as S bonds Au strongly and aids in the sintering of two Au NPs. The dimerization of two Au-$Fe_3O_4$ NPs was triggered by the fusion of two S-modified Au NPs at the reaction temperatures from 150°C to 200°C. Heating the non-S treated Au-$Fe_3O_4$ DBNPs under the same condition did not yield the $Fe_3O_4$-Au-$Fe_3O_4$ dumbbell structure.

### 2.2. DBNPs of Noble Metal (NM) and Quantum Dot (QD)

Strong chemical interactions between noble metal and S or Se element are often applied to synthesize DBNPs of NM and QDs. The synthesis may start with either QDs or NM NPs as seeds.

One early example is to grow Au NPs on CdSe nanorods to enhance the electric interconnect between the rods and the Au electrode.[13] The CdSe rods were prepared by high-temperature pyrolysis of dimethyl cadmium, $Cd(CH_3)_2$, and selenium trioctylphosphine, $SeP(C_8H_{17})_3$, in a solvent mixture containing trioctylphosphineoxide and phosphonic acid. Then $AuCl_3$ were dissolved in toluene in the presence of dodecyldimethylammonium bromide (DDAB) and dodecylamine. The CdSe nanorods were mixed with the Au solution at room temperature. After the reaction, the product was precipitated by addition of methanol and separated by centrifugation. Figure 6 shows the TEM images of the CdSe rod seeds (Figure 6a) and the composite Au-CdSe via controlled growth of Au onto the tips of CdSe quantum rods. The size of the Au NPs is controlled by the $AuCl_3$ concentration. The method for selective Au growth can be applied to various rod-like structures, including those with Au growing on each tip of the CdSe tetrapods[13] and on Pd nanorods via the galvanic replacement reaction between the nanorods and $[AuCl_4]^-$.[14]

Alternatively, Au-PbS or Au-PbSe NPs can be synthesized by mixing Au NPs with Pb-oleate and elemental S or Se solution followed by heating.[12] In the Au-PbS structure, Au was used to grow the second PbS on Au surface, forming PbS-Au-PbS ternary NPs.[12] The morphology was controlled primarily by the Au:S precursor ratio and the growth temperature. When the ratio of Au to S was high (1:10), nucleation of PbS on the Au surface depleted S, and only DBNPs were formed. When a lower Au to S ratio (1:20) was used, extra S remained present long enough to link and fuse the Au ends of two Au-PbS DBNPs into the PbS-Au-PbS structure.

The DBNPs of FePt-CdS were made from the core/shell FePt/CdS followed by dewetting of the CdS shell.[6] In the reaction solution after the growth of FePt NPs, elemental S was added. High affinity between FePt and S allowed S to be deposited on the surface of FePt, forming core/shell structured FePt/S. The subsequent addition of cadmium acetylacetonate, Cd $(acac)_2$, 1,2-hexadecanediol, and the surfactant trioctylphosphineoxide, produced metastable FePt/CdS NPs, where CdS was amorphous. Upon further annealing, the amorphous CdS crystallized, and the lattice mismatch between FePt and CdS crystals made the core/shell system metastable, leading to the formation of FePt–CdS DBNPs, as shown schematically in Figure 7. The extension of this synthesis led to the formation of $\gamma$-$Fe_2O_3$-MS (M = Zn, Cd, Hg) NPs where $\gamma$-$Fe_2O_3$ NPs were first made and used as seeds.[5]

Using the combination of the chemistry described above, more exotic DBNPs containing noble metal, magnetic NPs and QDs can be made. For example, PbS-Au-$Fe_3O_4$ NPs were obtained by mixing Au-$Fe_3O_4$ NPs with Pb-oleate complex and elemental S. Once S is added into the reaction flask containing the Pb-oleate complex and Au-$Fe_3O_4$ NPs, there is a competition between the adsorption of S onto the Au surface and reaction with the Pb-oleate to form PbS NPs. The competitive reaction leads to heterogeneous nucleation of PbS on the surface of the Au.[12] In the structure, Au NPs have typical plasmonic resonance and $Fe_3O_4$ NPs are superparamagnetic. But as seen in the section 3, the emission from the PbS NPs is severely quenched by Au due to the intimate contact between Au and PbS.

## 3. Optical and Magnetic Properties of DBNPs

Au and Ag NPs exhibit strong surface plasmon resonance (SPR) absorption, which is due to the collective oscillation of conduction electrons under an external electromagnetic field.[15] Semiconductor QDs often exhibit photoluminescence due to recombination of photo-excited carriers. Depending on the size, shape, composition and structure, magnetic NPs can be either ferromagnetic or superparamagnetic. The DBNPs integrate two or more such functionalities in a single entity. Depending on the interactions at the interface, both physical and chemical properties of each individual component in the DBNPs can be retained, enhanced or weakened.

The Au-$Fe_3O_4$ NPs show a red-shift in the Au SPR due to the intimate contact between Au and $Fe_3O_4$. Au NPs with sizes ranging from 5 to 20 nm in diameter often have a characteristic SPR at around 520 nm.[15] The exact absorption position varies with particle morphology and particle surface coating. Figure 8 is the UV-vis spectra of the Au and Au-$Fe_3O_4$ NPs dispersed in hexane. The peak at 520 nm for Au NPs is independent of the size and concentration of the NPs but the width increases with the decreased NP size (Figure 8a&b). However, once attached to $Fe_3O_4$, the Au NPs show SPR absorption at 538 nm (Figure 8c&d), a 18 nm red-shift from that of the pure Au NPs. As the dielectric environment for all the NPs in this measurement is the same, the only difference comes from the size and dumbbell-structure, this red-shift indicates that Au NPs in the DBNPs are electron deficient, which is likely caused by the interface communication between Au and $Fe_3O_4$. This is supported by our recent catalytic study on Au-$Fe_3O_4$ NPs in oxygen reduction reaction in which Au catalysis is enhanced upon the removal of $Fe_3O_4$ by acid etching.[16]

Compared with the Ag NPs dispersed in the same solvent, the Ag-$Fe_3O_4$ NPs show no SPR change.[9] This is due likely to the FeS-modification on the $Fe_3O_4$ surface during the synthesis. The presence of the thin (atomic) layer of sulfide between Ag and $Fe_3O_4$ may interrupt with electron transfer across the Ag-$Fe_3O_4$ interface, making the the SPR of Ag NPs unchanged.

Pure PbS NPs display strong quantum confinement, with the absorption edge tunable from 0.41 eV to 2.32 eV.[17] For example, the 8 nm PbS NPs showed intense photoluminescence (PL) at around 1750 nm. For DBNPs of 5 nm – 8 nm Au-PbS, the PL intensity was reduced by about a factor of 30 compared to the pure PbS NPs, as shown in Figure 9. This reduction is

not due to Au absorption of the excitation light as the quenching was similar using excitation wavelengths near 514 nm and 840 nm.[12] The conclusion is that the PL of PbS is severely quenched due to the intimate Au-PbS contact, which promotes charge separation across the interface between PbS and Au. This PL quench has been observed in other DBNPs of Au-CdSe,[13] Au-PbSe[12] and FePt-CdS[18] of different sizes and shapes. For the FePt-CdS DBNPs with FePt NP being 9 nm, the PL from CdS is completely quenched, but for the same DBNPs with FePt NP being 4 nm, the CdS NPs show clear band edge emission, although with an intensity reduced by a factor about 10 compared to the pure CdS NPs. Clearly, in the FePt-CdS structure, the emission reduction for CdS is FePt-size dependent.

In the NM-QD DBNPs, the influence of NM on the PL properties of the QD depends on the efficiency of charge transfer through NM-QD grain boundaries. Upon the direct contact between NM, such as Au and FePt, and QD, such as CdS, electrons tend to diffuse from the Fermi level of the NM to the conduction band of CdS. This leads to the downward band bending of CdS, causing charge accumulation at the interface, i.e. the formation of a Schotteky barrier. When electron-hole pairs are generated by photo-excitation in the semiconducting part, the electrons can transfer from CdS to Au or FePt but not vice versa due to the presence of this barrier. This leads to effective charge separation at the interface that prevents charge recombination within the semiconductor, leading to quenched emission. For very small metal NPs, however, due to the coulomb repulsion between electrons, the charging energy for adding extra electrons becomes very high. An estimate of a spherical metal NP with a radius of 2 nm and dielectric matrix of $\varepsilon = 2$ gives the charging energy of $\sim$ 0.4 eV. If the metal part cannot discharge into the surrounding media fast enough, the charge accumulates around the NP and the high charging energy prevents further electron transfer from the semiconducting part. The reduction of PL intensity is determined by the rate of electron-hole generation and the rate of discharging. The larger metallic domain leads to the stronger PL quenching of QD components. By tuning the size of the NM, it is possible to tune the QD emission in the NM-QD structure. Here the interplay between the quantum confinement and interface charge transfer determines the luminescence behavior of the QD NPs.

The interface communication between the nanoscale Au and $Fe_3O_4$ also leads to the change in magnetization behaviors of the magnetic NPs in the DBNP structures.[7] For Au-$Fe_3O_4$ NPs, Figure 10 shows the hysteresis loops measured at room temperature for Au-$Fe_3O_4$ particles with Au being 3 nm and $Fe_3O_4$ 14 nm (Figure 10a) and 6 nm (Figure 10b), respectively. Like $Fe_3O_4$ NPs, the DBNPs are superparamagnetic at room temperature. The 3–14 nm dumbbell particles show loops similar to the 14 nm $Fe_3O_4$ NPs with saturation moment reaching 80 emu/g, a value that is close to the related $Fe_3O_4$ NPs due to the negligible weight percentage of 3 nm Au in the composite. The 3–6 nm DBNPs, however, show a loop of slow increase in moment with the field up to 5 T (Figure 10b). As the pure $Fe_3O_4$ NPs in the same size do not show such a magnetization behavior, the slope is likely caused by surface spin canting of the small $Fe_3O_4$ NPs.[19] This spin canting is further aggravated upon the connection with Au NPs.[20]

The magnetic hysteresis loops of the 4 nm FePt-CdS and the 9 nm FePt-CdS NPs measured at 10 K show the reduced remanence ratio compared with the pure FePt NPs, indicating the weak exchange coupling between FePt and CdS.[18] However, there is no difference in coercivity between FePt NPs and FePt-CdS DBNPs. This is because the coercivity of FePt in FePt-CdS DBNPs is determined mainly by magnetocrystalline anisotropy of FePt, which is insensitive to slight surface modifications.

The DBNPs also show the interesting magneto-optical properties. Enhancement of magneto-optical response has been reported in composite thin-film multilayer metallic structures that combine a ferromagnetic film with a free-electron-like metal that augments the optical response

of the composite system.[21] A similar phenomenon has been observed in the DBNPs of Ag-$CoFe_2O_4$ in which $CoFe_2O_4$ is ferromagnetic at room temperature. Measuring the wavelength dependent Faraday rotation for the Ag-$CoFe_2O_4$ and $CoFe_2O_4$ NPs indicates that at short wavelengths the magnitude of the rotation and the shape of the hysteresis loops are comparable for the two types of particles (Figure 11a) due to the dominant effects by the $CoFe_2O_4$ interband transitions to the magneto-optical tensor in the highly absorptive violet/blue wavelength regime. However, a dramatic contrast emerges between the magneto-optical response for the Ag-$CoFe_2O_4$ and $CoFe_2O_4$ at longer wavelengths (Figure 11b) and the rotation becomes significantly enhanced for the DBNPs by nearly an order of magnitude near 633 nm. This strong contrast is due to the dielectric contribution of the Ag component in the Ag-$CoFe_2O_4$, which appears to produce a significant additive contribution to the overall magneto-optical response of the DBNPs.

## 4. DBNPs as catalyst

The DBNPs have similar structure feature to the supported NP catalyst except that the support itself is in nanometer scale. It is known that the catalytic behavior of the supported NPs is usually different from their individual counterparts. For example, Au NPs supported by proper oxides can have high catalytic activity for CO oxidation at low temperature, and many other oxidation reactions.[1,22] The enhanced Au catalysis is usually ascribed to the local modification of its electronic structures by the oxide support through the interface interaction. It is believed that the electronic structures of both metal and the oxide support are modified by electron transfer across the interface. As a result, electrons transfer from the support to the Fermi level of the adjacent Au, and give rise to oxygen vacancies on the surface of the oxide support that becomes active sites.[2] New study seems to indicate that small Au clusters are the real active source for catalysis.[1c] The small Au clusters have more low-coordinate Au atoms than do the extended Au crystal surfaces and have higher energy *d* states, which are more reactive and absorb/activate $O_2$ molecules more readily. This is further supported by a very recent microscopy study on an Au/$FeO_x$ catalyst system that the origin of the Au activity on CO oxidation is associated uniquely with Au bilayer clusters that are ~0.5 nm in diameter and contain ~10 Au atoms.[1f]

In the Au-$Fe_3O_4$ DBNPs, the epitaxial link between Au and $Fe_3O_4$ is established from the initial synthesis and the strong interface interactions make Au highly active for CO oxidation. In a recent demonstration,[23] the Au-$Fe_3O_4$ NPs were deposited on amorphous carbon supports and further calcined at 300°C in 8% $O_2$/He for 1 h to remove the residue of organic surfactant on the particle surface. The treated NPs showed significant activities for CO oxidation at room temperature. Figure 12 summarizes the light-off curves for CO oxidation catalyzed by Au-$Fe_3O_4$ NPs deposited on various supports. The reactivity shown on Au-$Fe_3O_4$/C is especially interesting as it is well-known that Au NPs loaded directly on the carbon supports are inactive for CO oxidation.[24] In contrast, the Au-$Fe_3O_4$ NPs supported on carbon are highly active for CO oxidation, showing 100% CO conversion at 50°C. This enhanced catalysis arises clearly from the local modification of the electronic structure of Au by $Fe_3O_4$ through the interface interaction.

The nanoscale effect is also present in a two metal DBNP system. The recent experimental results on Au clusters deposited on Pt NPs show that the interaction between Au and Pt modifies the Pt electronic structure toward a lower Pt surface energy, or lower-lying Pt *d*-band states. As a result, Au clusters have a stabilizing effect on the Pt surface under highly oxidizing conditions and suppress Pt dissolution during the $O_2$ reduction reaction (ORR) in acid without decreasing the oxygen reduction kinetics.[25] The epitaxial link between Pt and Au reduces the substantial loss of the Pt surface area over time in proton-exchange membrane fuel cells

condition and is particularly important for increased stability of the Pt electro-catalyst for the ORR at the cathode.

## 5. DBNPs as Dual Functional Imaging Probes for Biomedical Applications

The multi-functionality present within the DBNPs structure ensures that both magnetic and optical active NPs can be incorporated into one unit. The different NP surface also facilitates the controlled functionalization of each NP with a targeting agent or a therapeutic drug. These advantages make the DBNPs promising as multi-functional probes for diagnostic and therapeutic applications. DBNPs reported for such applications thus far are Au-$Fe_3O_4$,[3b] Ag-$Fe_3O_4$,[3a] Au-FePt[11] and CdSe-$Fe_2O_3$ NPs.[26] Here we use the Au-$Fe_3O_4$ NPs as an example to demonstrate the selected chemical modification of DBNPs as multifunctional probes for biomedical applications.

As synthesized, the Au-$Fe_3O_4$ DBNPs are coated with a layer of oleate and oleylamine. The NPs are made biocompatible by replacing the hydrophobic coating with a hydrophilic one. Figure 13a illustrates the surface functionalization of the 8–20 nm Au–$Fe_3O_4$ NPs. The original oleate/oleylamine coating on $Fe_3O_4$ is replaced by a catechol unit present in dopamine molecule that is linked to polyethylene glycol (PEG, Mr = 3000), and oleylamine around the Au NP is exchanged by HS-PEG-$NH_2$ (Mr = 2204) with HS attaching to Au. The epidermal growth factor receptor antibody (EGFRA) is linked to the PEG via EDC/NHS chemistry on the $Fe_3O_4$ side. Figure 13b is the TEM image of the NPs after surface modification. The antibody is used to target A431 cells that are known to over-express the epidermal growth factor receptor (EGFR).[27] Imaging EGFR over-expressed cells and tissues can potentially be used for early diagnostics and therapies of numerous cancers, including breast and lung cancers.[28]

The preferred binding between EGFR and EGFRA enabled the DBNPs to be populated on the surface or within the cytoplasm of A431 cells. MRI analyses revealed that A431 cells labeled with 8–20 nm Au–$Fe_3O_4$ NPs shorten the $T_2$ relaxation of the water molecules with relaxivity $r_1$ = 2.17/s mM and $r_2$ = 80.4/s mM. The $r_1$ is larger (but the $r_2$ is smaller) than that from the 20 nm $Fe_3O_4$ NPs (1.38/s mM and 121.13/s mM respectively), indicating the junction effect (reduced magnetization) in the dumbbell structure as described in Section 3, and cellular compartmentalization of the NPs that reduces proton relaxivity.[29]

A431 cells labeled with 8–20-nm Au–$Fe_3O_4$ NPs can also be visualized with a scanning confocal microscope at 594 nm, as shown in Figure 13c. The signal detected is from Au NPs in the DBNP structure and reflects the typical morphology of epithelial cells. It can be seen that the signal is much stronger in the region of cell–cell contact due to the preferred binding between EGFR and EGFRA. The Au NP-based optical probe is very stable and shows no signal loss after three days. This is extremely important for long-term tracking of the DBNPs in cellular environments. The detection limit for the 8–20-nm dumbbell is 90 pM Au. The experiments further reveal that that the reflection signal from the A431 cells incubated with the 8–20-nm Au–$Fe_3O_4$ NPs without EGFRA under the same concentration is much weaker, indicating that the EGFRA-labeled NPs have higher specificity in A431 cell targeting.

## 6. Conclusions

Recent synthetic progress has led to the controlled formation of DBNPs with two or more NPs in intimate contact. The interfacial interaction existed between two different NPs can indeed induce the change in physical and chemical properties of both NPs in the structure. Due to this interaction, the DBNPs have shown interesting catalytic, optical and magnetic properties. The distinct surface chemistry present in the DBNPs also facilitates the selected NP functionalization with either a targeting agent and/or a therapeutic agent, making these NPs especially important for target-specific medical diagnostic and therapeutic applications. These

previous research have demonstrated clearly that DBNPs are a new class of nanomaterials within which both physical and chemical properties can be tuned by controlling not only size, shape and composition of each individual NPs, but also interparticle interactions. They represent an exciting new nano-system and may provide what is needed to develop highly active catalysts for energy conversions and highly sensitive delivery probes for biomedical applications.

## References


1. a) Haruta M, Kobayashi T, Sano H, Yamada N. Chem. Lett 1987:405. b) Haruta M, Yamada N, Kobayashi T, Iijima S. J. Catal 1989;115:301. c) Chen MS, Goodman DW. Science 2004;306:252. [PubMed: 15331772] d) Hashmi ASK, Hutchings GJ. Angew. Chem. Int. Ed 2006;45:7896. e) Wang X, Na N, Zhang S, Wu Y, Zhang X. J. Am. Chem. Soc 2007;129:6062. [PubMed: 17458961] f) Herzing AA, Kiely CJ, Carley AF, Landon P, Hutchings GJ. Science 2008;321:1331. [PubMed: 18772433]
2. a) Molina LM, Hammer B. Phys. Rev. Lett 2003;90:206102. [PubMed: 12785908] b) Liu Z-P, Gong X-Q, Kohanoff J, Sanchez C, Hu P. Phys. Rev. Lett 2003;91:266102. [PubMed: 14754070] c) Laursen S, Linic S. Phys. Rev. Lett 2006;97:26101.
3. a) Gu H, Yang Z, Gao J, Chang CK, Xu B. J. Am. Chem. Soc 2005;127:34. [PubMed: 15631435] b) Xu C, Xie J, Ho D, Wang C, Kohler N, Walsh EG, Morgan JR, Chin YE, Sun S. Angew. Chem. Int. Ed 2008;47:173.
4. a) Murray CB, Kagan CR, Bawendi MG. Annu. Rev. Mater. Sci 2000;30:545. b) Cushing BL, Kolesnichenko VL, O'Connor CJ. Chem. Rev 2004;104:3893. [PubMed: 15352782]
5. Kwon K-W, Shim M. J. Am. Chem. Soc 2005;127:10269. [PubMed: 16028938]
6. Gu H, Zheng R, Zhang X, Xu B. J. Am. Chem. Soc 2004;126:5664. [PubMed: 15125648]
7. Yu H, Chen M, Rice PM, Wang SX, White RL, Sun S. Nano Lett 2005;5:379. [PubMed: 15794629]
8. Wang C, Daimon H, Sun S. Nano Lett. 2008 submitted.
9. a) Sun, S.; Wang, S.; Yu, H. US Patent. 7288134. b) Zhang L, Dou Y-H, Gu H-C. J. Colloid Interf. Sci 2006;297:660.
10. Li Y, Zhang Q, Nurmikko AV, Sun S. Nano Lett 2005;5:1689. [PubMed: 16159206]
11. Choi J, Jun Y, Yeon S-I, Kim HC, Shin J-S, Cheon J. J. Am. Chem. Soc 2006;128:15982. [PubMed: 17165720]
12. Shi W, Zeng H, Sahoo Y, Ohulchskyy TY, Ding Y, Wang ZL, Swihart M, Prasad PN. Nano Lett 2006;6:875. [PubMed: 16608302]
13. Mokari T, Rothenberg E, Popov I, Costi R, Banin U. Science 2004;304:1787. [PubMed: 15205530]
14. Camargo PHC, Xiong Y, Ji L, Zuo JM, Xia Y. J. Am. Chem. Soc 2007;129:15452. [PubMed: 18027954]
15. Daniel M-C, Astruc D. Chem. Rev 2004;104:293. [PubMed: 14719978]
16. Lee Y, Sun S. unpublished.
17. Wise FW. Acc. Chem. Res 2000;33:773. [PubMed: 11087314]
18. He S, Zeng H. J. Phys. Chem. C. 2008 in press.
19. Martinez B, Obradors X, Balcells L, Rouanet A, Monty C. Phys. Rev. Lett 1998;80:181.
20. Frey NA, Srinath S, Srikanth H, Wang C, Sun S. IEEE Tran. Magn 2007;43:3094.
21. a) Katayama T, Suzuki Y, Awano H, Nishihara Y, Koshizuka N. Phys. Rev. Lett 1988;60:1426. [PubMed: 10038035] b) Weller D, Reim W. Appl. Phys. Lett 1989;49:599.
22. a) Fu Q, Saltsburg H, Flytzani-Stephanopoulos M. Science 2003;301:935. [PubMed: 12843399] b) Zheng N, Stucky GD. J. Am. Chem. Soc 2006;128:14278. [PubMed: 17076500] c) Enache DI, Edwards JK, Landon P, Solsona-Espriu B, Carley AF, Herzing AA, Watanabe M, Kiely CJ, Knight DW, Hutchings GJ. Science 2006;311:362. [PubMed: 16424335]
23. Yin H, Wang C, Zhu H, Overbury SH, Sun S, Dai S. Chem. Comm 2008:4357. [PubMed: 18802569]
24. Ma Z, Liang CD, Overbury SH, Dai S. J. Catal 2007;252:119.
25. Zhang J, Sasaki K, Sutter E, Adzic RR. Science 2007;315:220. [PubMed: 17218522]

26. a) Selvan ST, Patra PK, Ang CY, Ying JY. Angew. Chem. Int. Ed 2007;46:2448. b) Gao J, Zhang W, Huang P, Zhang B, Zhang X, Xu B. J. Am. Chem. Soc 2008;130:3710. [PubMed: 18314984]

27. a) Haigler H, Ash JF, Singer SJ, Cohen S. Proc. Nat. Acad. Sci 1978;75:3317. [PubMed: 356052] b) Kawamoto T, Sato JD, Le A, Polikoff J, Sato GH, Mendelsohn J. Proc. Nat. Acad. Sci 1983;80:1337. [PubMed: 6298788]

28. a) Adams GP, Weiner LM. Nature Biotech 2005;23:1147. b) Herbst RS. Int. J. Rad. Onc. Bio. Phys 2004;59:21.

29. Simon GH, Bauer J, Saborovski O, Fu YJ, Corot C, Wendland MF, Daldrup-Link HE. Eur.Radiol 2006;16:738. [PubMed: 16308692]

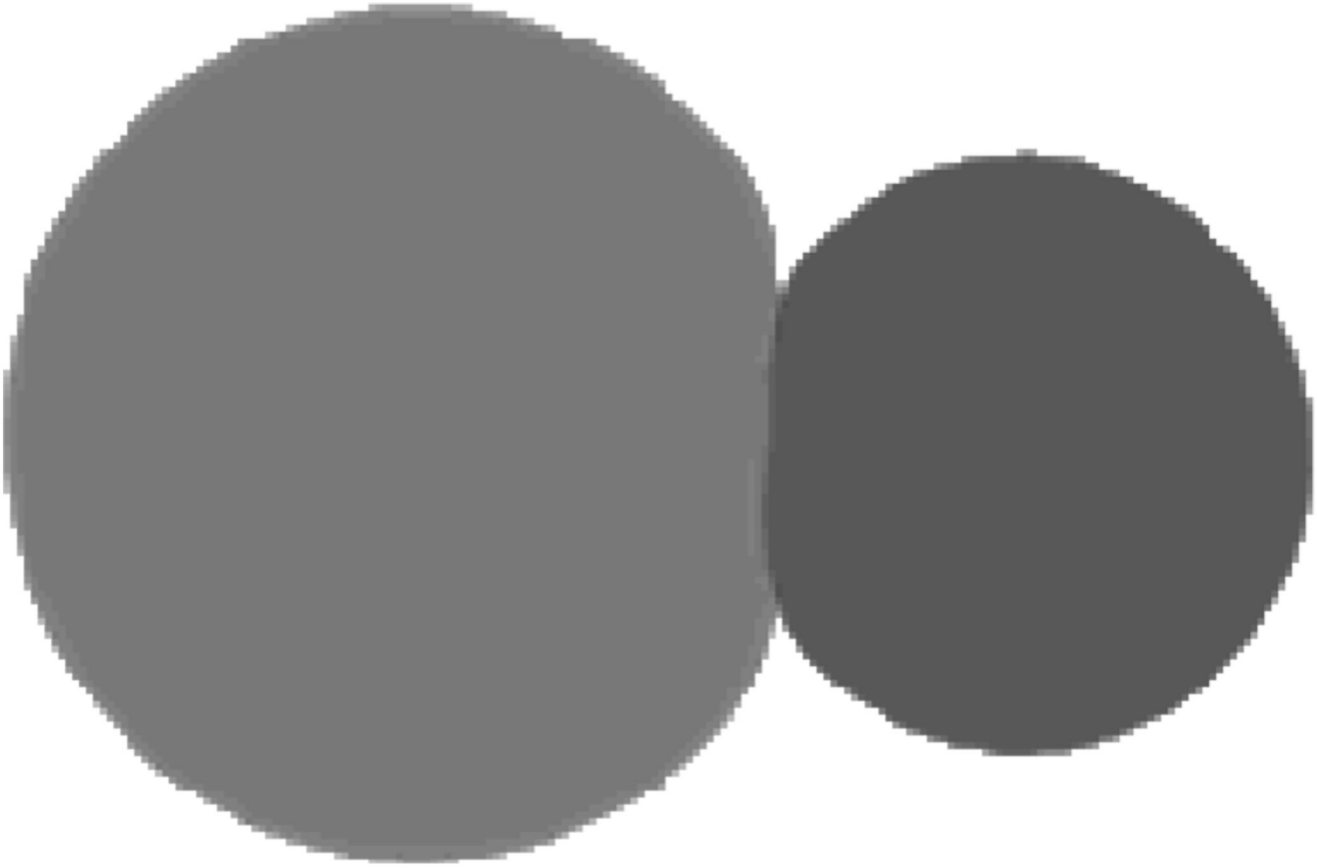

**Figure 1.**
Schematic illustration of a dumbbell-like nanoparticle sturcture described in this reveiw.

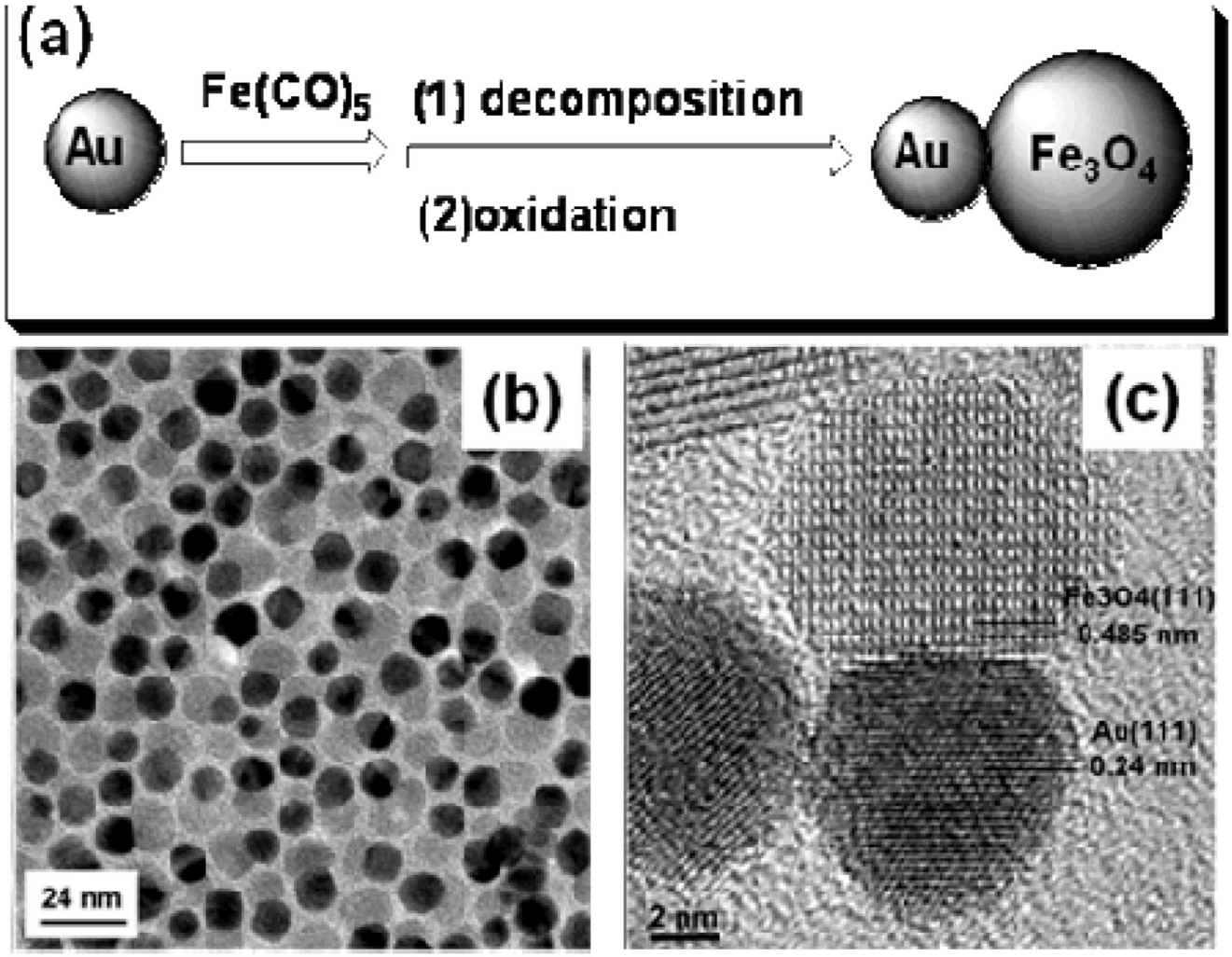


**Figure 2.**
(a) Schematic illustration of the growth of Au-$Fe_3O_4$ DBNPs. (b) TEM and (c) HRTEM images of the 8 nm – 14 nm Au-$Fe_3O_4$ DBNPs. Reproduced with permission from reference [7].

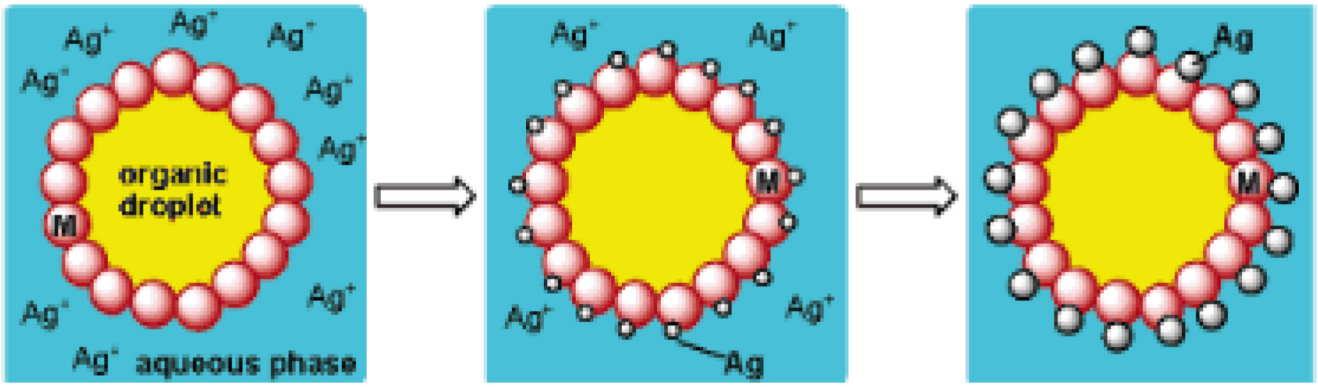


**Figure 3.**
Schematic illustration of the formation of DBNPs in a micellar structure by ultrasonication of a heterogeneous solution with as-prepared $Fe_3O_4$ NPs in the organic phase and $AgNO_3$ in water. Reproduced with permission from reference [3a].

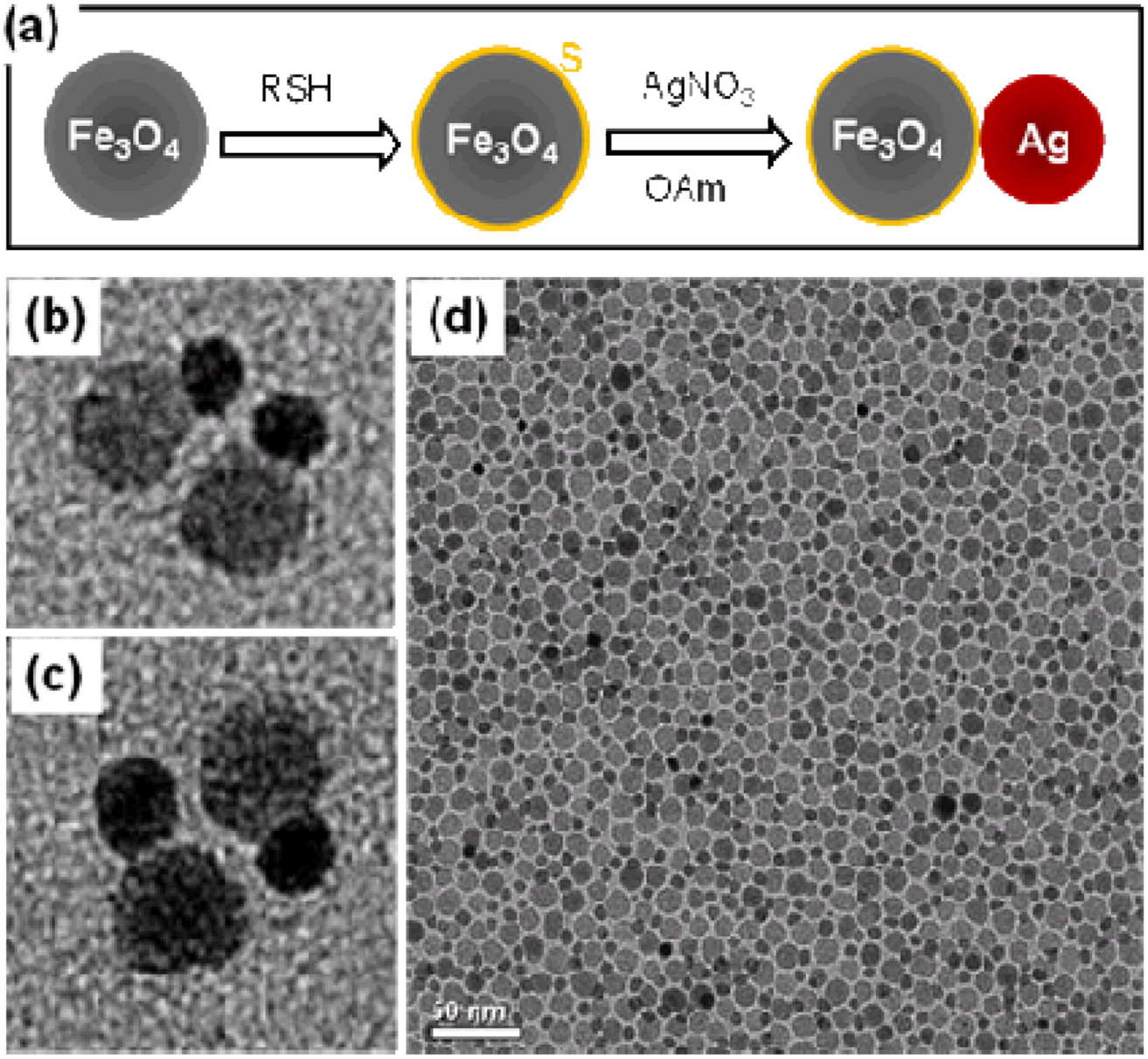


**Figure 4.**
(a) Schematic illustration of the syntehsis of Ag-$Fe_3O_4$ DBNPs and TEM images of the two Ag-$Fe_3O_4$ DBNPs aligned parallel (b), antiparallel (c) and an assembly of Ag-$Fe_3O_4$ NPs.

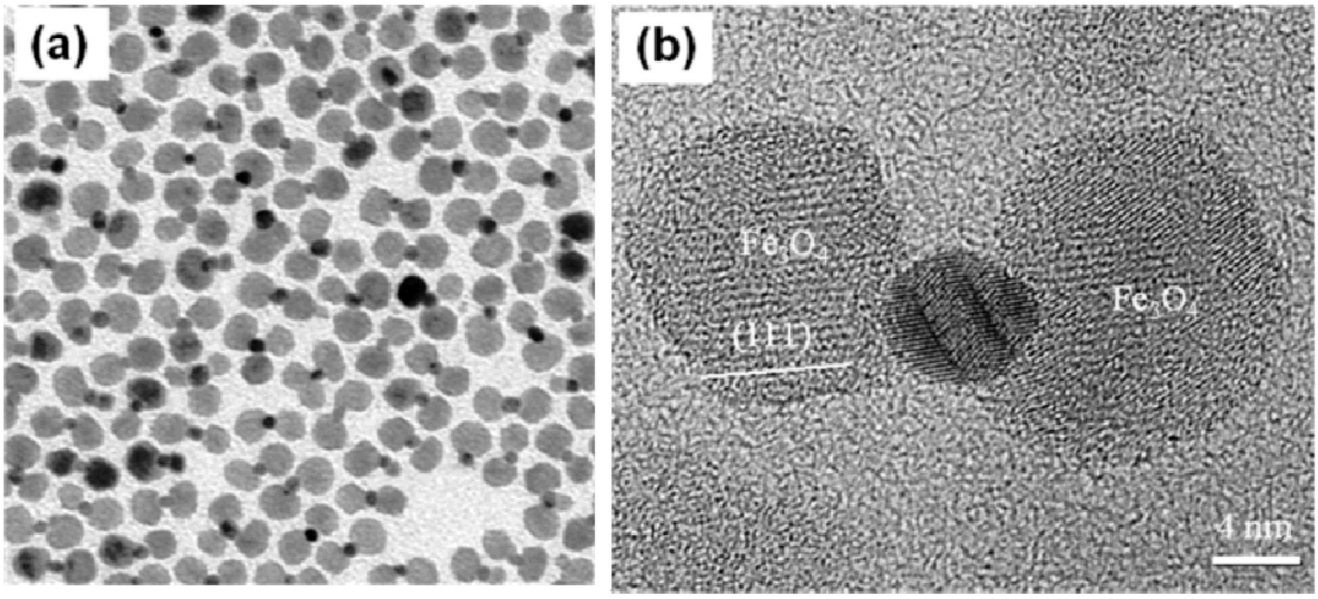


**Figure 5.**
(a) TEM and (b) HRTEM images of $Fe_3O_4$-Au-$Fe_3O_4$ DBNPs. Reproduced with permission from reference [12].

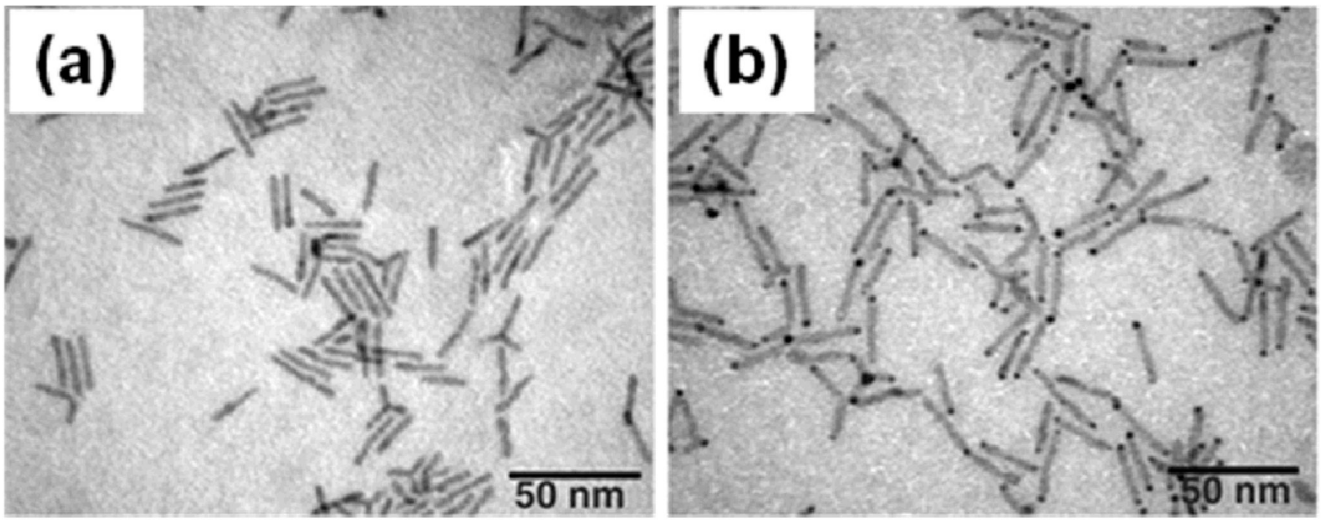


**Figure 6.**
TEM images of (a) Au nanorods (29 × 4 nm) and (b) Au-CdSe composite NPs with CdSe growing on the tip of the Au nanorods. Reproduced with permission from reference [13].

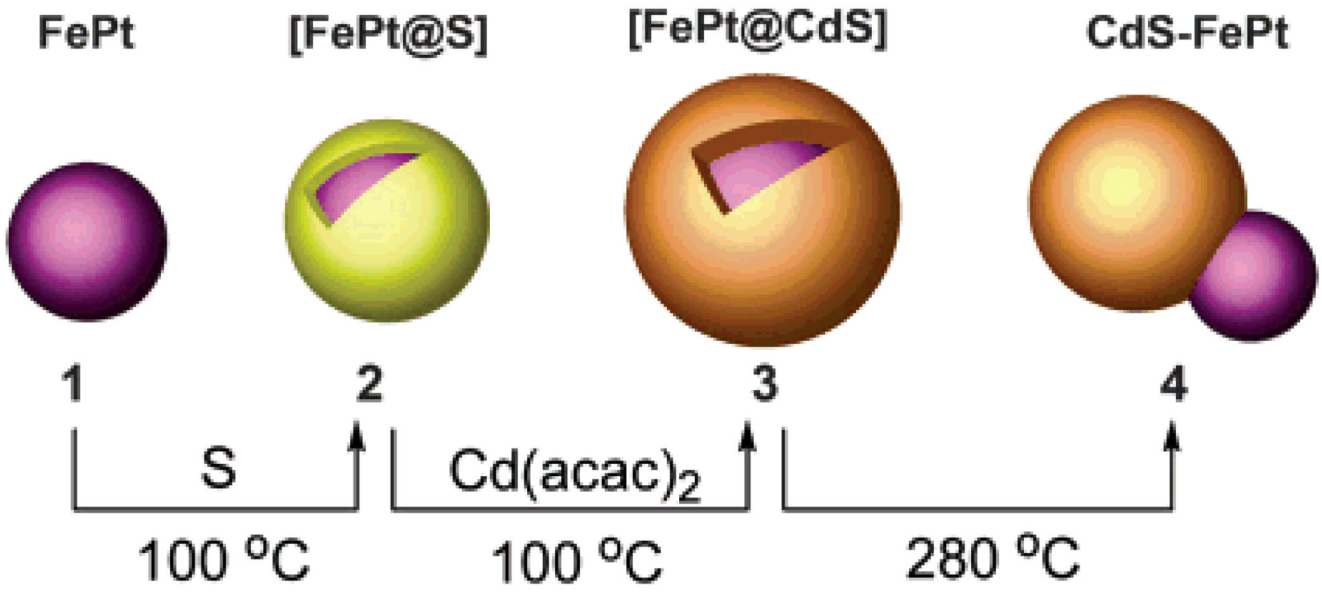


**Figure 7.**
Schematic illustration of the formation of CdS-FePt DBNPs. Reproduced with permission from reference [6].

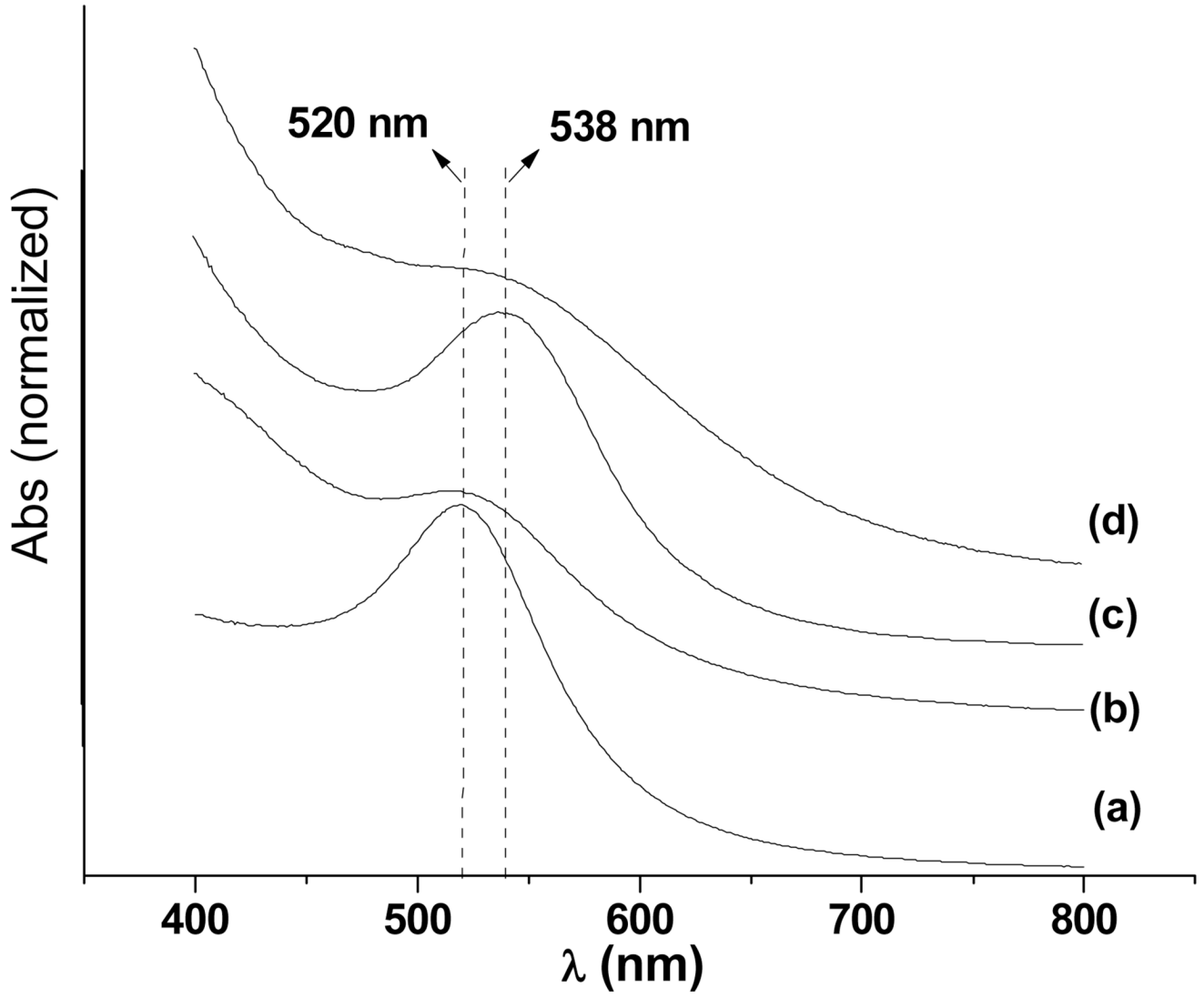


**Figure 8.**
UV-Vis spectra of the Au and Au-$Fe_3O_4$ NP dispersions in hexane: (A) 8 nm Au; (B) 4 nm Au; (C) 7 nm–14 nm Au-$Fe_3O_4$; and (D) 3 nm–14 nm Au-$Fe_3O_4$. Reproduced with permission from reference [7].

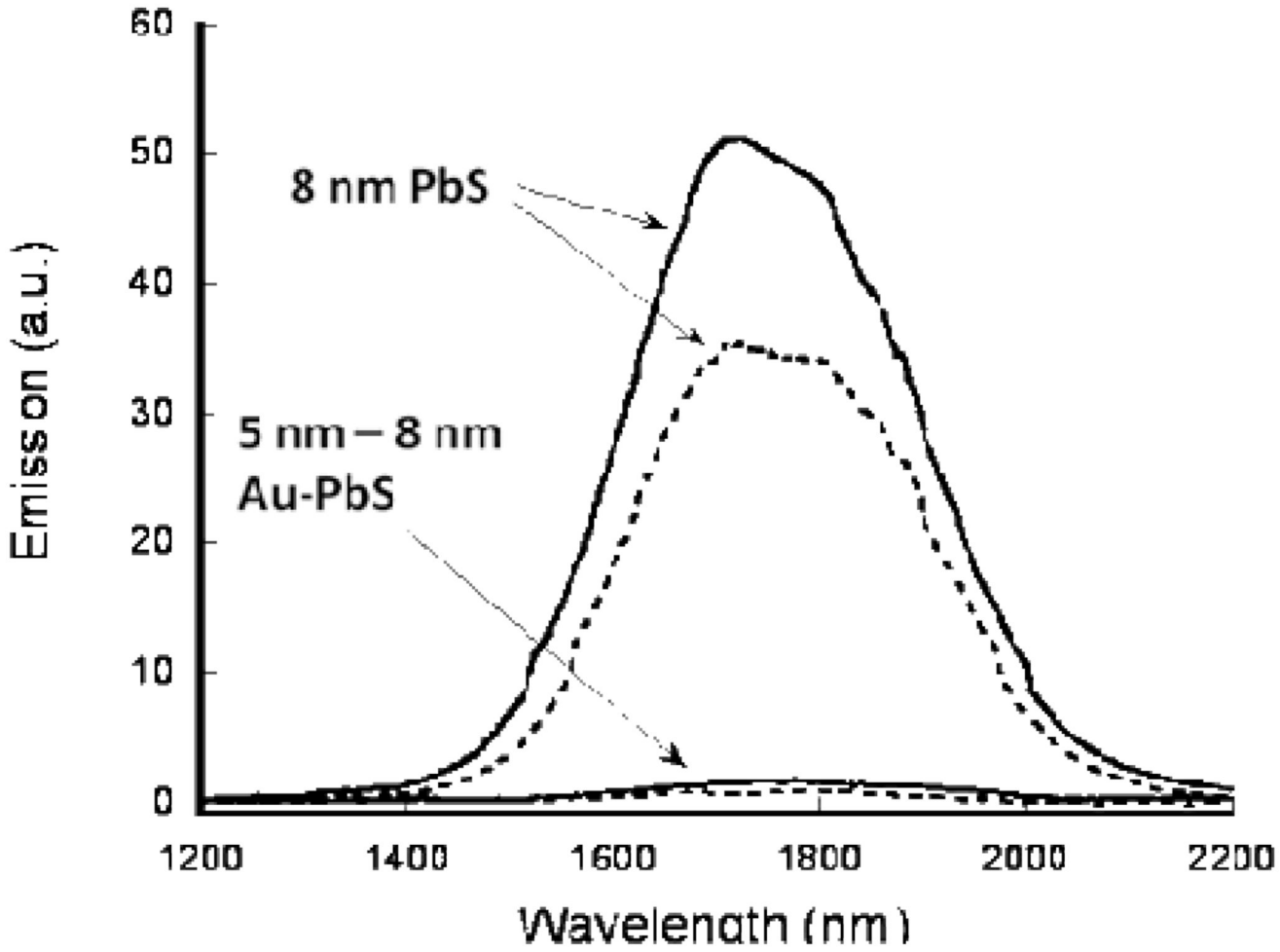


**Figure 9.**
The photoluminescence spectra for PbS and Au-PbS DBNPs. PL quenching is observed in the DBNPs, compared to pure PbS NPs. The emission data are shown as solid curves for 514 nm excitation, and dashed curves for 840 nm excitation. Reproduced with permission from reference [12].

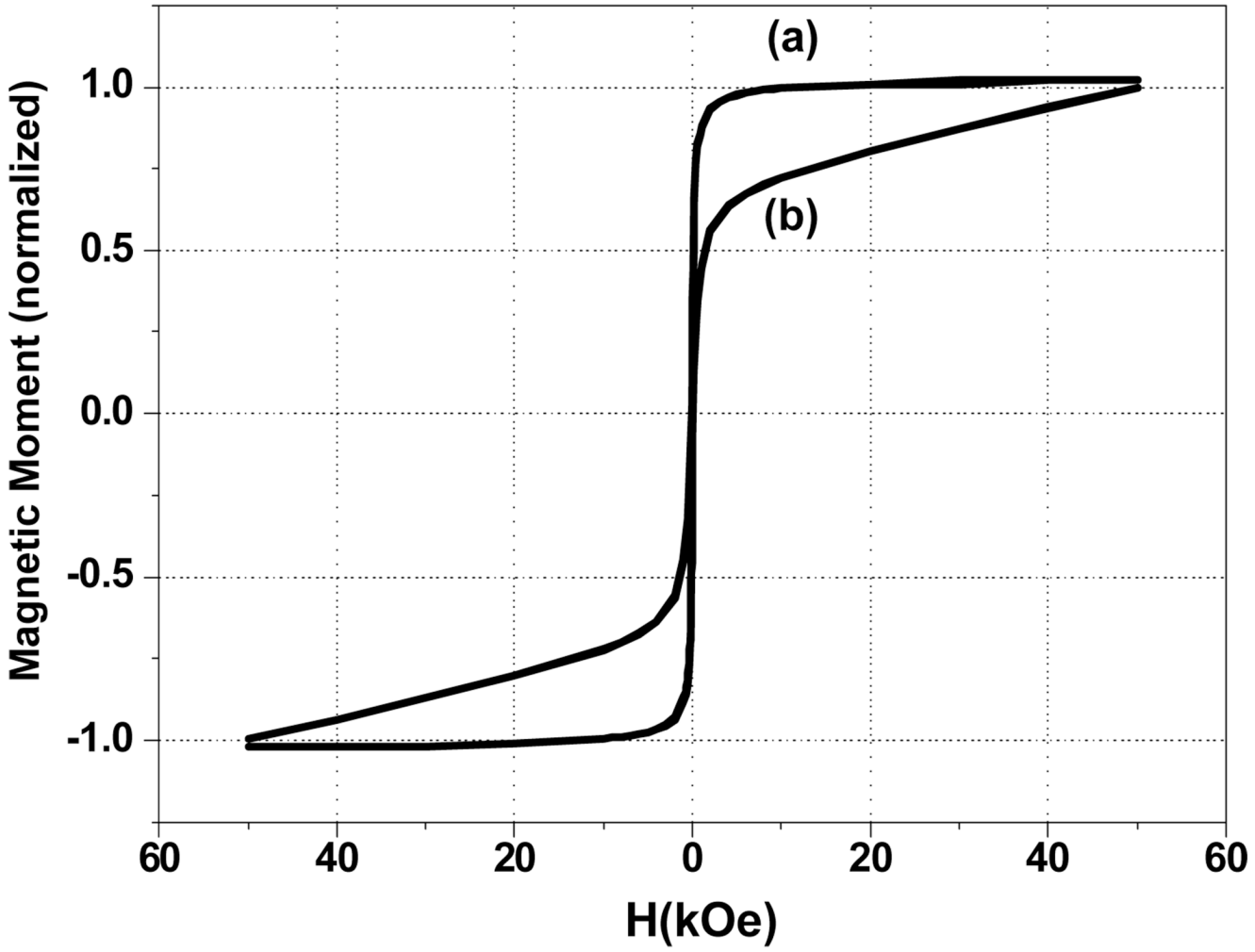


**Figure 10.**
Hysteresis loops of the Au-$Fe_3O_4$ DBNPs measured at room temperature: (a) 3 nm–14 nm Au-$Fe_3O_4$ and (b) 3 nm–6 nm Au-$Fe_3O_4$ NPs. Reproduced with permission from reference [7].

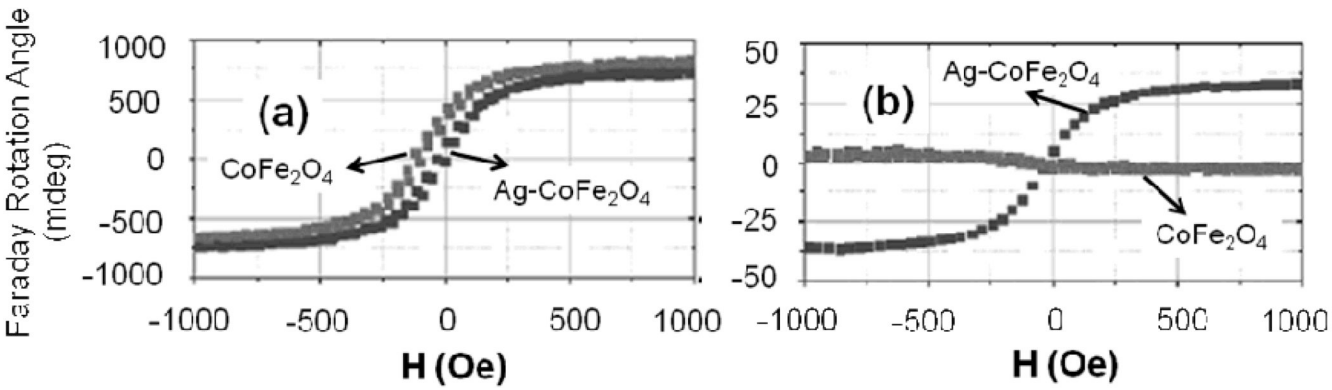


**Figure 11.**

Magnetooptical Faraday rotation of Au-$CoFe_2O_4$ NPs and $CoFe_2O_4$ NPs in hexane at laser wavelengths of (a) 385 nm, and (b) 633 nm, respectively, (~100 nM concentration; optical path length is 2 mm). Reproduced with permission from reference [10].

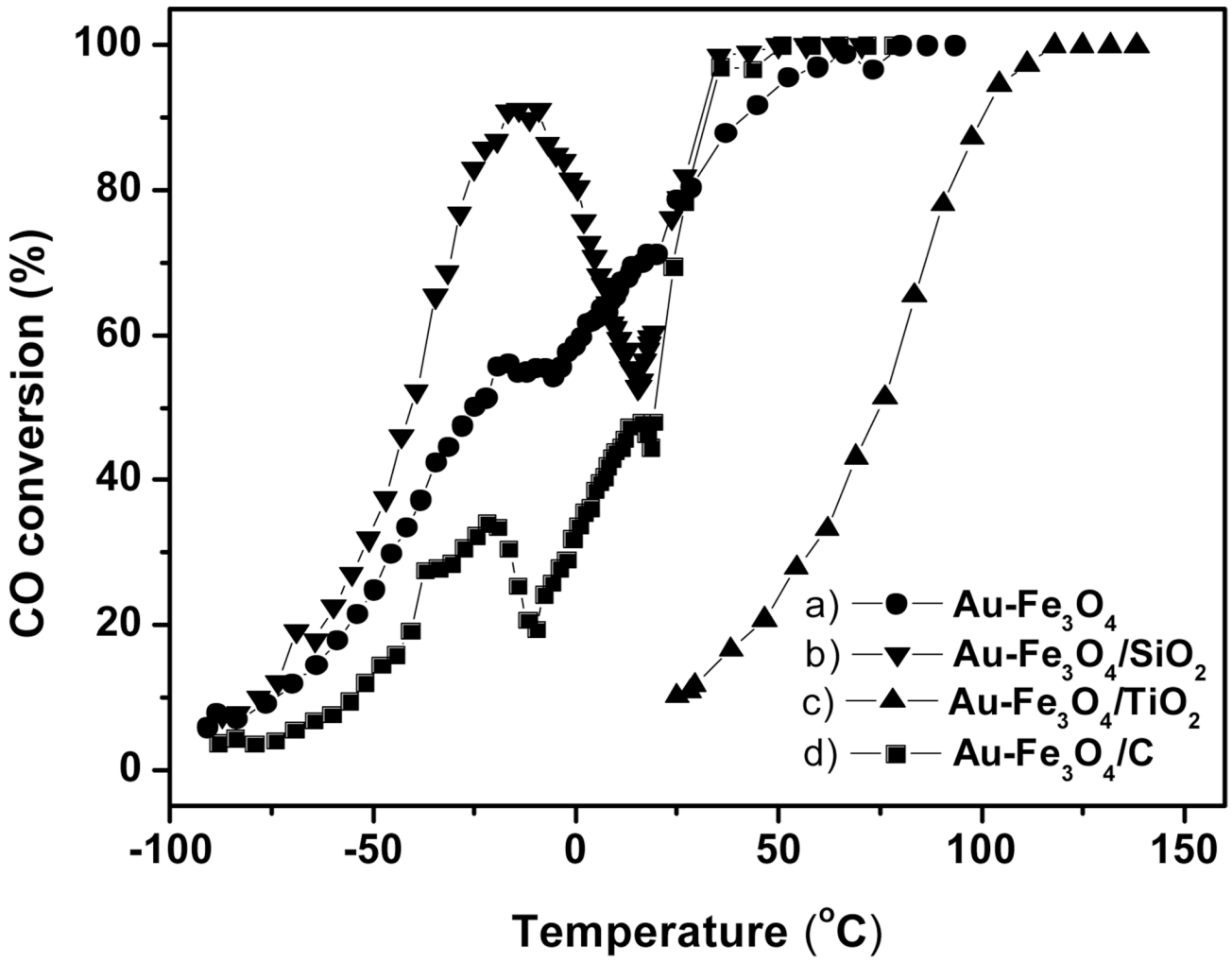


**Figure 12.**
CO oxidation conversion light-off curves of Au-$Fe_3O_4$ deposited on $SiO_2$, $TiO_2$ and carbon: a) Au-$Fe_3O_4$: Au-$Fe_3O_4$ nanoparticles calcined at 300 °C for 1h; b) Au-$Fe_3O_4$/$SiO_2$: Au-$Fe_3O_4$ deposited on $SiO_2$ was calcined at 500 °C for 1h; c) /Au-$Fe_3O_4$/$TiO_2$: Au-$Fe_3O_4$ deposited on $TiO_2$ was calcined at 300 °C for 1h; d) Au-$Fe_3O_4$/C: Au-$Fe_3O_4$ deposited on carbon was calcined at 300 °C for 1h. Reproduced with permission from reference [22].

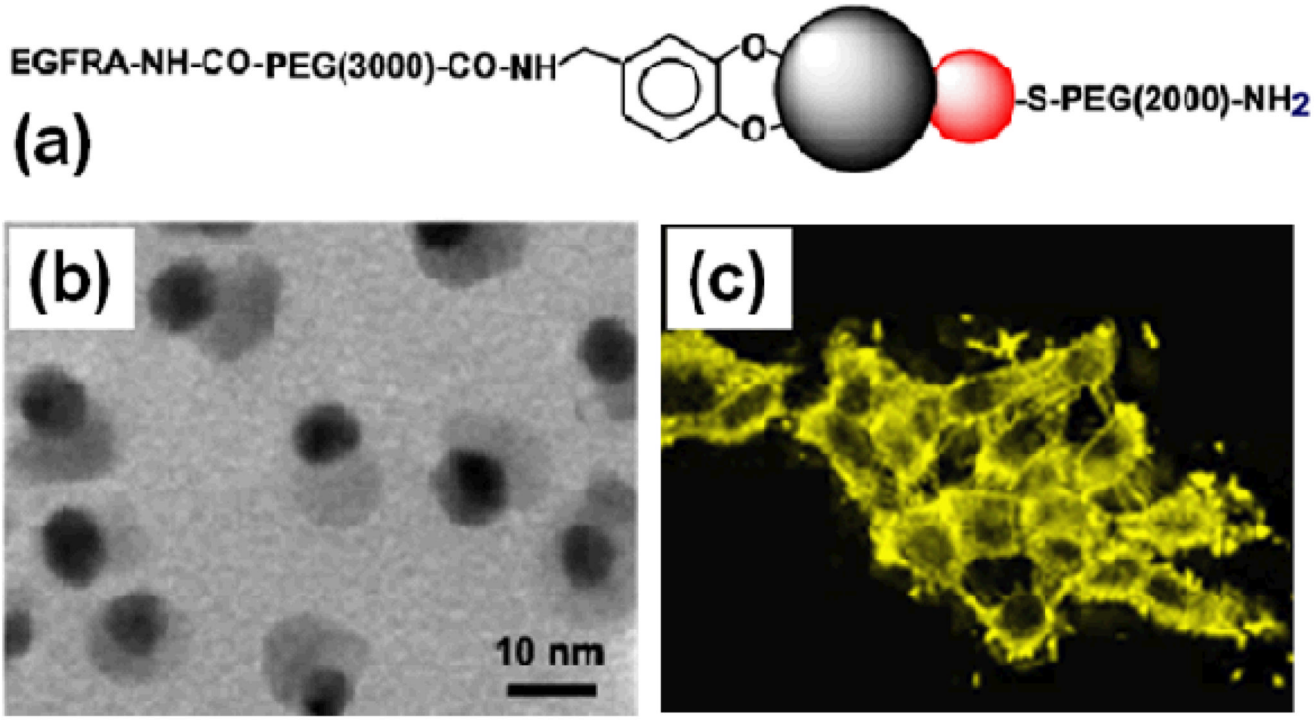


**Figure 13.**
(a) Schematic illustration of surface functionalization of the Au-$Fe_3O_4$ DBNPs, (b) TEM image of the 8 nm – 20 nm Au-$Fe_3O_4$ NPs after surface modification, (c) Reflection images of the 8 nm – 20 nm Au-$Fe_3O_4$ labeled A431 cells. Reproduced with permission from reference [3b].